

Using Diffusion Models to do Data Assimilation

Daniel Hodyss¹ and Matthias Morzfeld²

¹ Remote Sensing Division, Naval Research Laboratory, Washington DC

² Cecil H. and Ida M. Green Institute of Geophysics and Planetary Physics, Scripps Institution of Oceanography, University of California, San Diego, CA

Abstract

The recent surge in machine learning (ML) methods for geophysical modeling has raised the question of how these same ML methods might be applied to data assimilation (DA). We focus on diffusion modeling (generative artificial intelligence) and on systems that can perform the *entire* DA, rather than on ML-based tools that are used within an otherwise conventional DA system. We explain that there are (at least) three different types of diffusion-based DA systems and we show in detail that the three systems differ in the type of posterior distribution they target for sampling. The different posterior distributions correspond to different priors and/or likelihoods, which in turn results in different types of training data sets, different computational requirements and different accuracies of their state estimates. We discuss the implications of these findings for the use of diffusion modeling in DA.

1 Introduction

Data assimilation (DA) is a mathematical and computational framework for updating forecasts in view of observations (see, e.g., [Kalnay, 2002](#)). Mathematically, DA relies on Bayes’ rule and all numerical methods for DA can be understood as approximating, in one way or another, a Bayesian posterior distribution. In numerical weather prediction (NWP), we distinguish between Monte Carlo based, ensemble Kalman methods (see, e.g., [Anderson, 2001](#); [Evensen, 1994](#); [Evensen et al., 2009](#); [Tippett et al., 2003](#)), optimization-based/variational methods (see, e.g., [Talagrand and Courtier, 1987](#)), and “hybrid” methods that combine the Monte Carlo approach with optimization (see, e.g., [Buehner et al., 2013](#); [Hamill and Snyder, 2000](#); [Kuhl et al., 2013](#); [Lorenc, 2003](#); [Poterjoy and Zhang, 2015](#); [Zhang et al., 2009](#)). Collectively, we will refer to these methods as “conventional DA,” since these methods have been deployed in NWP for the past few decades with great success.

Recently, there has been an enormous surge in machine learning (ML) methods as applied to geophysical modeling (see, e.g., [Kochkov et al., 2024](#); [Lam et al., 2023](#); [Price et al., 2025](#)), which has raised the question of how these same ML tools might be used within or even replace a conventional DA system. The obvious first step might be to replace the physics-based forecast model with a data-driven ML version (see, e.g., [Adrian et al., 2025](#)) while continuing to employ conventional DA methods. A more ambitious step is to replace the entire conventional DA system via ML, e.g., using a diffusion model, which is a form of generative artificial intelligence (AI) and will be discussed further below, (see, e.g., [Chung et al., 2023](#); [Li et al., 2025](#); [Manshausen et al., 2024](#); [Pathak et al., 2024](#); [Qu et al., 2024](#); [Rozet and Louppe, 2023](#)), through other ML methods (see, e.g., [Allen et al., 2025](#)) or even in the absence of a training set ([Keller and Potthast, 2024](#)).

In this paper we concentrate on the question: *in what ways can a diffusion model replace the entire conventional DA system?* We will argue that the answer to this question can be understood by considering subtleties in Bayes’ rule and the different ways of formulating a Bayesian posterior distribution. Briefly, a conventional DA system samples a Bayesian posterior distribution constructed

from a prior that is time-dependent and potentially modified by the entire past trajectory of observations. This observation-dependent prior propagates information from previous DA cycles to the current cycle, and we will refer to it as a *cycling prior* for short. In contrast, we will show that the common practice of using a training set derived from a long time-series of past weather to train diffusion DA algorithm’s samples a different Bayesian posterior distribution with a constant, *climatological* prior. In some cases, diffusion DA systems attempt to bring in additional information, beyond the observations, in the form of a “forecast,” either generated by the diffusion DA or by other means, but we will show that this is still not equivalent to the posterior distribution obtained using a cycling prior. We are then left to conclude that, except in rare circumstances (Bao et al. (2024)), conventional DA and diffusion DA target *different* posterior distributions. We feel that a key question that needs to be answered is: *which of these posterior distributions is best in the sense that it has the smallest variance?* The answer to this question reveals, at least in principle, which algorithmic choices have the best possibility of producing state estimates with the lowest error along with accurate probabilistic inference.

On the other hand, whether a particular DA method is better than another also depends on whether one can accurately sample from that particular posterior distribution *in practice*. The nonlinearity of the dynamical system being predicted often means that the relevant prior and posterior are non-Gaussian, which implies the potential for significant error in sampling that posterior using conventional DA algorithms that make Gaussian assumptions (Morzfeld and Hodyss (2019)). Hence, in practice the degree of nonlinearity can obscure the differences between the different posterior distributions alluded to above, especially when it is likely that diffusion DA algorithms may be more adept at handling non-Gaussianity than conventional DA. We do not attempt to answer questions about the impact of non-Gaussianity on the differences between these methods because the answer is clearly application dependent. Instead, we focus entirely on explaining the differences between the various possible algorithmic choices in terms of precisely identifying the particular formulation of Bayes’ rule each method is attempting to solve. We emphasize that this identification of which Bayes’ rule each method is attempting to solve will transcend the differences between linear and nonlinear systems as well as any differences between Gaussian and non-Gaussian distributions. Consequently, we will assume that each method is able to accurately sample its own version of Bayes’ rule and the only question left is then about the differences between the various forms of Bayes’ rule. We therefore leave the description of the impact of non-Gaussianity and the application dependent differences between all these methods to future work.

To this end, we focus on a simplified, linear example that is amenable to analysis and analytical expressions (no approximations). Specifically, we show how variants of diffusion DA systems target different Bayesian posterior distributions, defined by different prior distributions and/or likelihoods. We then construct various training sets that imply these distinctly different diffusion models. This process allows us to broadly assess the main differences between various diffusion DA systems and conventional DA.

Our main results are:

1. Traditional diffusion DA is effective at sampling a Bayesian posterior distribution with a fixed, climatological prior, but the accuracy of such a system is inferior to a DA system that samples a Bayesian posterior distribution with a time-evolving cycling prior. Again, whether this result is borne out in practice is likely to strongly depend on the degree of nonlinearity, time between observations, quantity and quality of the observations, etc.
2. A diffusion DA system can sample the exact same posterior distribution as a DA system using

a time-evolving cycling prior, but the denoiser in such a diffusion DA system will need to be re-trained at each DA cycle, which incurs a significant computational cost.

3. A diffusion DA system with a fixed, climatological prior can be modified to ingest a forecast in addition to the observations. This forecast appears to add some aspects of the time-evolving cycling prior back into the DA system, but is not entirely equivalent. Furthermore, if this forecast is generated by a separate DA system, the training cost is relatively low and the accuracy is higher than that of a DA system with a climatological prior (but without a forecast). Nevertheless, the resulting accuracy of this extended diffusion DA system that additionally uses a forecast is lower than that of a DA system with a cycling prior.

While these results are rigorous, they directly apply only to a simplified linear system and in the limits of a large training set (for diffusion DA) and a large ensemble size (for conventional DA). Nonetheless, the Bayesian posterior distributions we connect to the different variants of diffusion DA systems generalize to any setup using the same broad algorithmic choices for the diffusion model. We will argue that we can learn a lot from this knowledge of the targeted posterior distributions and that this will allow us to draw practically relevant conclusions.

The rest of this paper is organized as follows. In Section 2 we will introduce both conventional and diffusion-based DA systems. In Section 3 we describe a linear, stochastic dynamical system that will allow us to clearly formulate all aspects of the DA problem analytically. We will apply different forms of diffusion-DA systems to this dynamical model in order to reveal the prior, likelihood and posterior each system corresponds with. In Section 4 we provide a numerical illustration of the main results from Section 3. We close the manuscript with a summary of the major results and their conclusions in Section 5.

2 Conventional and diffusion-based data assimilation

We begin by briefly introducing the fundamental aspects of both conventional DA and diffusion modeling. Our focus here is on revealing how each method samples a different Bayesian posterior distribution.

2.1 Conventional data assimilation

Data assimilation is concerned with approximating a time-evolving Bayesian posterior distribution that describes the probability of a system state \mathbf{x}_k at (discrete) time k , given observations $\mathbf{y}_1, \mathbf{y}_2, \dots, \mathbf{y}_{k-1}, \mathbf{y}_k$ up to time k :

$$p(\mathbf{x}_k | \mathbf{y}_1, \dots, \mathbf{y}_k) \propto p(\mathbf{y}_k | \mathbf{x}_k) p(\mathbf{x}_k | \mathbf{y}_1, \dots, \mathbf{y}_{k-1}). \quad (1)$$

It is important to note here that information is propagated from cycle-to-cycle by a time evolving prior. In other words, the posterior of the previous cycle is used to generate the prior for the next cycle. For the remainder of this paper we will thus refer to the prior $p(\mathbf{x}_k | \mathbf{y}_1, \dots, \mathbf{y}_{k-1})$ as a *cycling* prior. Various DA algorithms approximate the above Bayesian posterior distribution in one way or another. Here, we use the ensemble Kalman filter (EnKF) (Burgers et al., 1998; Evensen, 1994; Evensen et al., 2009) as a representative example of a conventional DA system. In preparation for the diffusion modeling to come, we emphasize that the EnKF takes in a training set, referred to in the literature as an “ensemble”, and outputs a new training set that is used at the next cycle.

This regeneration step of the EnKF works as follows. At cycle $k - 1$, we have observations $\mathbf{y}_1, \dots, \mathbf{y}_{k-1}$ and samples from $p(\mathbf{x}_{k-1} | \mathbf{y}_1, \dots, \mathbf{y}_{k-1})$ in the form of an ensemble $\mathbf{x}_{k-1}^{(i)}$, where super-

script $i = 1, \dots, n_e$ indexes the ensemble members (and n_e is the ensemble size). The EnKF makes a *forecast* for time k by evolving the ensemble $\mathbf{x}_{k-1}^{(i)}$ forward in time using the model; the result is a forecast ensemble, viz.

$$\mathbf{x}_{fk}^{(i)} = \mathcal{M}(\mathbf{x}_{k-1}^{(i)}), \quad (2)$$

where $\mathcal{M}(\cdot)$ is a forecast model (physics-based or ML/AI). This forecast ensemble represents the prior, $p(\mathbf{x}_k | \mathbf{y}_1, \dots, \mathbf{y}_{k-1})$, as a collection of samples. The forecast ensemble is updated to an *analysis* ensemble by employing stochastic ensemble generation (van Leeuwen (2020)), viz.

$$\mathbf{x}_{ak}^{(i)} = \mathbf{x}_{fk}^{(i)} + \mathbf{K}(\mathbf{y}_{k+1} - (\mathbf{H}\mathbf{x}_{fk}^{(i)} + \boldsymbol{\varepsilon}^{(i)})), \quad (3)$$

where we assume for ease of presentation that the observation operator is linear, i.e.,

$$\mathbf{y}_k = \mathbf{H}\mathbf{x}_k + \boldsymbol{\varepsilon}, \quad (4)$$

where $\boldsymbol{\varepsilon}$ is a Gaussian random variable with mean 0 and covariance matrix \mathbf{R} ; $\boldsymbol{\varepsilon}^{(i)}$ in (3) is a sample from the same distribution as $\boldsymbol{\varepsilon}$; the matrix

$$\mathbf{K} = \mathbf{P}\mathbf{H}^T(\mathbf{H}\mathbf{P}\mathbf{H}^T + \mathbf{R})^{-1}, \quad (5)$$

is an ensemble approximation of the Kalman gain and \mathbf{P} is the ensemble covariance (usually localized (see Morzfeld and Hodyss (2023)) and inflated (see Whitaker and Hamill (2012), Hodyss et al. (2016), Gharamti et al. (2019))).

2.2 Diffusion modeling

The goal in diffusion modeling is to construct a procedure to sample a random variable with probability density function (pdf), $p(\mathbf{x})$, given a sufficiently large number of samples from that distribution in the form of a training set. This training set plays an identical role to the ensemble in the EnKF above. The main distinction between the ensemble in Section 2.2.1 and the training set here is that the training set is never updated with the latest information from observations, but the ensemble of Section 2.2.1 is updated with that information. This distinction will be relaxed in Section 3.3.2.3.2.2 where we develop a diffusion model that does update its training set at each cycle.

The standard approach in diffusion modeling is to set up a forward process in the form of a simple stochastic differential equation (SDE) and to then reverse that process. In the forward process, we start with a sample from $p(\mathbf{x})$ and sequentially add noise to the sample. These steps are then reversed, so that we can obtain a sample from $p(\mathbf{x})$. A neural network is trained on the samples (and the successively noisy versions of it) to enable the reverse process. Once trained, the diffusion model takes in noise and outputs a sample from the desired pdf.

Below we will refer to the state of the forward process with, \mathbf{u} , and the state of the reverse process with, \mathbf{v} . We employ a very simple forward process following Karras et al. (2022), i.e.,

$$d\mathbf{u} = \sqrt{2t}d\beta_t, \quad (6)$$

where the initial conditions for (6) are drawn from $p(\mathbf{x})$ and where β_t is a standard Brownian motion (i.e. a Wiener process).

This approach is referred to as a “variance-exploding” method because the variance of (6) monotonically increases with time. The solution to (6) has the property that

$$\mathbf{u}_t | \mathbf{u}_0 \sim N(\mathbf{u}_0, t^2), \quad (7)$$

which means that the samples from this pdf are created by simply adding Gaussian noise to samples drawn from $p(\mathbf{x})$. This is an extremely important property as we will use (7) to make use of Tweedie’s formula (Efron (2011)) as discussed below.

Given the forward process (6), we have, according to Anderson (1982), a reverse process that is integrated backwards in time (from $t = T$ to $t = 0$):

$$d\mathbf{v} = -2t\nabla \log(p_t(\mathbf{v}))dt + \sqrt{2t}d\bar{\beta}_t \quad (8)$$

where $p_t(\mathbf{v})$ is the time evolution of the marginal pdf of (6) and $\bar{\beta}_t$ is a reverse-time Brownian motion. Therefore, we generate the i^{th} sample from $p(\mathbf{x})$ as $\mathbf{x}^{(i)} = \mathbf{v}(t = 0)$.

Note that the time, t , in both (6) and (8) are not model or physical time. Rather, the parameter, t , is to be thought of as, just that, a parameter denoting the virtual time within the diffusion model. In any event, given the highly noisy nature described by (7) we draw the initial condition for (8) from a Gaussian with mean zero and variance T^2 where T is a large final virtual time of which we imagine the forward process stopped.

The term $\nabla \log p_t(\mathbf{v})$ is referred to as the “score function” and we use Tweedie’s formula (see Appendix A) to compute this as

$$\nabla \log p_t(\mathbf{v}) = \frac{E_{\mathbf{x} \sim p(\mathbf{x}|\mathbf{v}_t)}[\mathbf{x}] - \mathbf{v}_t}{t^2}, \quad (9)$$

where the expectation in (9) is shorthand for

$$E_{\mathbf{x} \sim p(\mathbf{x}|\mathbf{v}_t)}[\mathbf{x}] = \int_{-\infty}^{\infty} \mathbf{x}p(\mathbf{x}|\mathbf{v}_t)d\mathbf{x} \quad (10)$$

Recall that the conditional expectation $E_{\mathbf{x} \sim p(\mathbf{x}|\mathbf{v}_t)}[\mathbf{x}]$ is the best estimate in the sense of mean-square of \mathbf{x} for a given \mathbf{v} . We can thus calculate the expected value required in (9) by a “denoiser”, $D(\mathbf{v}_t, t)$, that minimizes a loss function defined from the expected mean squared error, i.e.,

$$\ell = E_{\mathbf{x} \sim p(\mathbf{x})}E_{n \sim \mathcal{N}(0, t^2)}\|\mathbf{x} - \mathbf{D}(\mathbf{v} = \mathbf{x} + n, t)\|_2^2 \quad (11)$$

where $\|\cdot\|_2^2$ denotes the L_2 norm. In practice, the denoiser is a neural network that is trained to predict \mathbf{x} from \mathbf{v}_t . The training set is as follows. For each sample \mathbf{x} , we have noisy versions at various times in the forward process, which we can obtain by simply adding noise to the sample \mathbf{x} according to the rule defined by (7). These “sample” and “noisy sample” pairs are used to train the denoiser. Once trained, we can use the denoiser to simulate the reverse process:

$$d\mathbf{v} = -2\frac{D(\mathbf{v}, t) - \mathbf{v}}{t}dt + \sqrt{2t}d\bar{\beta}_t. \quad (12)$$

The reverse process now allows us to sample the desired pdf, $p(\mathbf{x})$, by initializing the reverse process with white noise and simulating it backwards in virtual time.

2.3 Diffusion-based data assimilation

Diffusion modeling, as outlined just above, is an ML technique that samples a random variable by fitting a stochastic differential equation (SDE) to a training set (Sohl-Dickstein et al. (2015), Ho et al. (2020)). There is a very large literature on diffusion modeling. A common extension

of the description of diffusion modeling given above is conditional image generation in which one generates images of a requested scene given text prompts (see, e.g., [Ding et al., 2025](#); [Zhan et al., 2024](#)).

This type of conditional image generation using diffusion modeling is precisely what is required for DA. The typical approach is to reuse the tried-and-true recipe from generating images, i.e., we train a diffusion model to take in noise and then generate (atmospheric) system states. The only difference to the diffusion model outlined in Section 2.2.2 is that we condition on the *current* set of observations, \mathbf{y}_k , i.e., the denoiser is the minimizer of the loss function

$$\ell = E_{\mathbf{x}_k, \mathbf{y}_k \sim p(\mathbf{x}_k, \mathbf{y}_k)} E_{n \sim \mathcal{N}(0, t^2)} \|\mathbf{x}_k - \mathbf{D}(\mathbf{v} = \mathbf{x}_k + n, \mathbf{y}_k, t)\|_2^2, \quad (13)$$

where $p(\mathbf{x}_k, \mathbf{y}_k)$ is the *joint* posterior and this conditioning is well-understood in the diffusion modeling literature (see, e.g., [Batzolis et al., 2021](#); [Chung et al., 2023](#); [Qu et al., 2024](#)).

Note that the procedure goes like this: we collect a large set of training data in the form of a time-series of system states \mathbf{x}_k and observations \mathbf{y}_k . We subsequently set up a denoiser in the form of a neural network to minimize the loss function in (13). This training is once and for all and (usually) never repeated. The result is a diffusion model that takes in the latest observations and then generates an atmospheric system state. Examples of the use of diffusion models that work in this way include [Chung et al. \(2023\)](#); [Li et al. \(2025\)](#); [Manshausen et al. \(2024\)](#); [Pathak et al. \(2024\)](#); [Qu et al. \(2024\)](#); [Rozet and Louppe \(2023\)](#), but the list of papers is rapidly expanding.

We will show below that we can interpret the output of such a diffusion model as samples from the following pdf:

$$p(\mathbf{x}_k | \mathbf{y}_k) \propto p(\mathbf{y}_k | \mathbf{x}_k) p(\mathbf{x}_k), \quad (14)$$

where the training set corresponds to samples from the prior, $p(\mathbf{x}_k)$, i.e., the training set is a long time-series of past weather. Note that the above posterior distribution is different from the posterior distribution in (1) used in conventional DA. The key difference lies in the prior. For diffusion DA, the prior is implicitly defined by the training dataset, which is not updated from cycle-to-cycle and, thus, will be referred to here as a *climatological* prior. This implies that this climatological prior is independent of observations from the recent past. This form of DA with a climatological prior is unusual from the perspective of conventional DA because conventional DA has always valued the cycling nature of the DA problem and has therefore traditionally focused on the posterior distribution (1) using a cycling prior.

Other variants of diffusion DA supplement the observations \mathbf{y}_k with an additional predictor in the form of a forecast, \mathbf{f}_k , either produced by the diffusion DA or by other means (see, e.g., [Huang et al., 2024](#)). We will show below that since the prior corresponds to the training set (which is again not cycled in these works), the forecast is implicitly treated like an additional observation. Hence, the targeted posterior distribution in these works is

$$p(\mathbf{x}_k | \mathbf{y}_k, \mathbf{f}_k) \propto p(\mathbf{y}_k, \mathbf{f}_k | \mathbf{x}_k) p(\mathbf{x}_k). \quad (15)$$

The forecast is a function of all past observations, but the prior is not updated and remains climatological (assuming no *re-training* at each DA cycle). Instead, the likelihood is modified to incorporate the forecast as a kind of additional observation. Such DA systems are thus somewhat in between a cycling, conventional DA system and the diffusion DA described just above with a climatological prior. We will label DA systems that incorporate a forecast as an *extended likelihood* DA system, because the observations are *extended* to include the forecast and this extended set of observations are then used within a likelihood as in (15).

2.4 Other forms of ML assisted data assimilation

Our focus here is on diffusion DA and on answering questions related to how generative AI may be able to replace an entire ensemble DA system and what it might mean if it does. But ML methods have other uses in DA which we want to briefly acknowledge. Perhaps most importantly, there is a flurry of recent activity on using, for example, the ERA5 reanalysis for training ML-based *forecast* models (see, e.g., Kochkov et al., 2024; Lam et al., 2023; Li et al., 2024; Mardani et al., 2025; Price et al., 2025). In terms of probability distributions, these ML methods sample conditional distributions of the type

$$p(\mathbf{x}_{k+T}|\mathbf{x}_k, \mathbf{x}_{k-1}), \quad (16)$$

where T is the desired forecast lead time and where we (arbitrarily) stopped the conditioning two time steps backwards in time (as, e.g., GenCast does, Price et al. (2025)). In terms of DA, these ML-based forecast models can be used as the model in these systems, but then the conventional DA system is still required. In this sense, ML-forecasting as part of a cycling DA system is very different from the diffusion DA systems we study here, because we have chosen to only consider diffusion models that aim at replacing the DA system, i.e., retain the forecast model unchanged. Experiments with replacing the physics-based forecast model with ML type models within an ensemble DA system are currently ongoing (see, e.g., Adrian et al., 2025).

3 Diffusion modeling in a linear, stochastic dynamical system

We illustrate here how a diffusion DA system emulates various forms of Bayesian posterior distributions by considering a linear, stochastic dynamical system for which we can compute the various posterior distributions without approximation using the Kalman filter formalism. The model describes the time evolution of an n_x -dimensional state, \mathbf{x} , governed by the stochastic differential equation (SDE)

$$d\mathbf{x} = -\frac{1}{2}\mathbf{x}ds + d\beta_s \quad (17)$$

where β_s is a standard Wiener process and s denotes physical time. Observations \mathbf{y}_k are collected Δs time units apart via a linear observation operator, \mathbf{H} , generating n_y observations at each observation time

$$\mathbf{y}_k = \mathbf{H}\mathbf{x}_k + \boldsymbol{\varepsilon}_k. \quad (18)$$

where $\boldsymbol{\varepsilon}_k$ is a draw from $N(\mathbf{0}, r\mathbf{I})$. To keep the analysis simple, \mathbf{H} is composed of rows of the identity matrix, i.e., we observe n_y components of \mathbf{x} directly.

The climatological prior for this problem is obtained from a long simulation of the dynamics, (17). For a diffusion DA system, this long model run is used as the training set. One reason we chose this simple problem setup is that we know the climatological prior analytically. For the linear dynamics (17), we can compute the climatological prior by solving the corresponding steady-state Fokker-Planck equation

$$\nabla \circ \left(\frac{1}{2}\mathbf{x}p \right) + \frac{1}{2}\nabla^2 p = 0, \quad (19)$$

with the boundary condition that the function $p(\mathbf{x})$ vanishes at $|\mathbf{x}| \rightarrow \infty$. The solution is the standard Gaussian, i.e.,

$$p(\mathbf{x}) = \frac{1}{(2\pi)^{\frac{n_x}{2}}} \exp \left(-\frac{1}{2}\mathbf{x}^T \mathbf{x} \right). \quad (20)$$

Note that similar, uncorrelated Gaussians have been used extensively to study conventional DA systems (see, e.g., Bengtsson et al., 2008; Bickel et al., 2008; Hodyss and Morzfeld, 2023; Morzfeld and Hodyss, 2023; Snyder et al., 2008, 2015).

3.1 DA with a climatological prior

We now sample the Bayesian posterior distribution with a climatological prior. We first consider the Kalman approach in order to compute the moments of the posterior distribution analytically. We then show that the typical training paradigm used in diffusion modeling leads to this same result.

3.1.1 Bayesian posterior

We can use the Kalman filter to compute the exact mean and covariance of the posterior distribution with a climatological prior (20). Since this posterior distribution is Gaussian, we only need to compute the posterior mean and posterior covariance. Using the fact that the climatological prior has mean zero and the identity covariance matrix, we find

$$\bar{\mathbf{x}}_k^a = \mathbf{H}^T [\mathbf{H}\mathbf{H}^T + r\mathbf{I}]^{-1} \mathbf{y}_k, \quad (21)$$

$$\mathbf{P}^a = \mathbf{I}_N - \mathbf{H}^T [\mathbf{H}\mathbf{H}^T + r\mathbf{I}]^{-1} \mathbf{H}, \quad (22)$$

for the posterior mean and covariance. Since we assume that \mathbf{H} only contains a subset of the rows of the identity matrix, there is no correlation between the state variables and we can examine the posterior mean element-wise and consider only the diagonal elements of the posterior covariance matrix. For an observed grid-point, we have

$$[\mathbf{x}_k^a]^j = \frac{1}{1+r} y, \quad (23)$$

$$[\mathbf{P}^a]^{jj} = 1 - \frac{1}{1+r} = \frac{r}{1+r}. \quad (24)$$

where $y = [\mathbf{y}_k]^j$ is shorthand notation for the j^{th} element of the observation vector, \mathbf{y}_k . Note that the posterior covariance is independent of the observations.

3.1.2 Diffusion DA

To setup a diffusion DA system for this problem, we use the forward process (6) and thus integrate

$$d\mathbf{v} = -2t\nabla \log(p_t(\mathbf{v}|\mathbf{y}_k))dt + \sqrt{2t}d\bar{\beta}_t \quad (25)$$

backward in virtual time (from $t = T$ to $t = 0$).

We use Tweedie's formula

$$\nabla \log p_t(\mathbf{v}|\mathbf{y}_k) = \frac{E_{\mathbf{x}_k \sim p(\mathbf{x}_k|\mathbf{v}, \mathbf{y}_k)}[\mathbf{x}_k] - \mathbf{v}}{t^2}, \quad (26)$$

to compute the score, but avoid neural networks. Rather, we use the fact that the conditional expectation in (26) is the minimum of

$$\ell = E_{\mathbf{x}_k, \mathbf{y}_k \sim p(\mathbf{x}_k, \mathbf{y}_k)} E_{n \sim \mathcal{N}(0, t^2)} \|\mathbf{x}_k - \mathbf{D}(\mathbf{v} = \mathbf{x}_k + n, t, \mathbf{y}_k)\|_2^2, \quad (27)$$

Note that we have

$$p(\mathbf{x}_k, \mathbf{y}_k) = p(\mathbf{y}_k | \mathbf{x}_k) p(\mathbf{x}_k) \quad (28)$$

which represents a joint posterior distribution using a climatological pdf. This implies that the training set consists of samples from a long simulation of the dynamical system under consideration paired up with observations at each time in the training set.

The minimum of (27) for a linear, Gaussian problem is a kind of Kalman filter of the form

$$\mathbf{D}(\mathbf{v}, t, \mathbf{y}_k) = E_{\mathbf{x}_k \sim p(\mathbf{x}_k | \mathbf{v}, \mathbf{y}_k)}[\mathbf{x}_k] = \hat{\mathbf{H}}^T [\hat{\mathbf{H}} \hat{\mathbf{H}}^T + \mathbf{R}]^{-1} \hat{\mathbf{y}} \quad (29)$$

where

$$\mathbf{R} = \begin{bmatrix} t^2 \mathbf{I}_{n_x} & \mathbf{0} \\ \mathbf{0} & r \mathbf{I}_{n_o} \end{bmatrix}, \quad \hat{\mathbf{H}} = \begin{bmatrix} \mathbf{I}_{n_x} \\ \mathbf{H} \end{bmatrix}, \quad \hat{\mathbf{y}} = \begin{bmatrix} \mathbf{v} \\ \mathbf{y}_k \end{bmatrix}. \quad (30)$$

Using the Kalman formalism here allows us to obtain analytical expressions for both the denoiser and the score. On the other hand, in practice one would obtain very similar results with a well-trained denoiser. In this sense, replacing the denoiser with equation (29) is equivalent to assuming that the diffusion model is trained on an essentially infinite training dataset.

The diffusion model thus becomes

$$d\mathbf{v} = -\frac{2}{t} \left[\hat{\mathbf{H}}^T [\hat{\mathbf{H}} \hat{\mathbf{H}}^T + \mathbf{R}]^{-1} \hat{\mathbf{y}} - \mathbf{v} \right] dt + \sqrt{2t} d\bar{\beta}_t \quad (31)$$

Note that the “effective” observation error covariance in (30) implies that, early in the reverse process ($t^2 \gg r$), the state is drawn towards the observations, \mathbf{y}_k , but when $t^2 \ll r$, the state is drawn towards \mathbf{v} . Similarly, note that the noise term vanishes as $t \rightarrow 0$ but the drift term takes on a greater significance. These two effects ensure that the ensemble obtained from the diffusion model has the correct mean and variance.

The simple observation operator we consider here implies that there is no covariance between state variables, and thus we can consider a single element of the vector \mathbf{v} , which we call v for simplicity. For an observed element of \mathbf{v} at the i^{th} gridpoint we have

$$dv = -\frac{2}{t} \left[\frac{\frac{r}{1+r}}{\frac{r}{1+r} + t^2} v + \frac{\frac{t^2}{1+r}}{\frac{r}{1+r} + t^2} y - v \right] dt + \sqrt{2t} d\bar{\beta}_t \quad (32)$$

This equation can be solved analytically (see Appendix B):

$$v(0) = \frac{\frac{r}{1+r}}{\frac{r}{1+r} + T^2} v(T) + \frac{r}{(1+r)^2} \frac{T^2}{\frac{r}{1+r} + T^2} y + \frac{r}{1+r} \int_T^0 \frac{\sqrt{2t}}{\frac{r}{1+r} + t^2} d\bar{\beta}_t \quad (33)$$

Note that $v(0)$ is the random variable of interest and we can compute its mean as

$$\langle v(0) \rangle = \frac{\frac{r}{1+r}}{\frac{r}{1+r} + T^2} \langle v(T) \rangle + \frac{r}{(1+r)^2} \frac{T^2}{\frac{r}{1+r} + T^2} y. \quad (34)$$

In the limit $T \rightarrow \infty$ we find

$$\langle v(0) \rangle_{T \rightarrow \infty} = \frac{1}{1+r} y \quad (35)$$

which is the posterior mean we obtained via the Kalman filter in (23), i.e., without diffusion.

Similarly, we can compute the variance

$$\langle (v(0) - \langle v(0) \rangle)^2 \rangle = \frac{\frac{r}{1+r}}{\frac{r}{1+r} + T^2} (v(T) - \langle v(T) \rangle)^2 + \left\langle \left(\frac{r}{1+r} \int_T^0 \frac{\sqrt{2t}}{\frac{r}{1+r} + t^2} d\bar{\beta}_t \right)^2 \right\rangle \quad (36)$$

where we have used the fact that the cross-term vanishes. The stochastic integral on the right-hand side requires the use of the Itô isometry, i.e.,

$$\begin{aligned} \left\langle \left(\int_T^0 \frac{\sqrt{2t}}{\frac{r}{1+r} + t^2} d\bar{\beta}_t \right)^2 \right\rangle &= \left\langle \left(- \int_0^T \frac{\sqrt{2t}}{\frac{r}{1+r} + t^2} d\bar{\beta}_t \right)^2 \right\rangle \\ &= 2 \int_0^T \frac{t}{(\frac{r}{1+r} + t^2)^2} dt = -2 \int_T^0 \frac{t}{(\frac{r}{1+r} + t^2)^2} dt \end{aligned} \quad (37)$$

Finally, we find the variance to be

$$\langle (v(0) - \langle v(0) \rangle)^2 \rangle = \frac{\frac{r^2}{(1+r)^2} T^2}{(\frac{r}{1+r} + T^2)^2} + \frac{r}{1+r} \frac{T^2}{\frac{r}{1+r} + T^2} \quad (38)$$

which in the limit as $T \rightarrow \infty$ becomes

$$\langle (v(0) - \langle v(0) \rangle)^2 \rangle_{T \rightarrow \infty} = \frac{r}{1+r}, \quad (39)$$

which is the same variance we obtained via the Kalman filter in (24).

Hence, we have now shown that the use of a long time-series of samples from a dynamical system as a training set for a diffusion model results in a diffusion DA system that samples a Bayesian posterior distribution constructed with a climatological prior.

3.2 DA with a cycling prior

We now consider the more conventional DA approach of sampling the Bayesian posterior distribution (1), with a cycling prior that propagates information from one cycle to the next.

3.2.1 Bayesian posterior

For our simplified linear example in which the observation network and observation error variance is fixed in time, it is well-known that the forecast covariance, analysis (posterior) covariance and Kalman gain converge to a steady-state, i.e., $\mathbf{P}^f \rightarrow \mathbf{P}_\infty^f$, $\mathbf{P}_a \rightarrow \mathbf{P}_\infty^a$, $\mathbf{K} \rightarrow \mathbf{K}_\infty$ and therefore we have that

$$\mathbf{P}_\infty^a = (\mathbf{I} - \mathbf{K}_\infty \mathbf{H}) \mathbf{P}_\infty^f, \quad (40)$$

$$\mathbf{K}_\infty = \mathbf{P}_\infty^f \mathbf{H}^T (\mathbf{H} \mathbf{P}_\infty^f \mathbf{H}^T + r \mathbf{I})^{-1}. \quad (41)$$

The posterior mean at time k is

$$\bar{\mathbf{x}}_{ak} = \bar{\mathbf{x}}_{fk} + \mathbf{K}_\infty (\mathbf{y}_k - \mathbf{H} \bar{\mathbf{x}}_{fk}), \quad (42)$$

where $\bar{\mathbf{x}}_{fk}$ is the forecast mean, i.e., the posterior mean of the previous cycle evolved forward using an ensemble under the dynamics (17) to the next observation time. Note that our focus

on the steady-state here can be understood as having completed sufficiently many cycles with a well-constructed conventional DA system.

Since our observation system is simple (direct observations of n_y elements of \mathbf{x}_k), it is again sufficient to focus on one observed variable from the state vector. Denoting the j^{th} diagonal element of \mathbf{P}_∞^f by α_j we obtain an expression for the j^{th} element of the analysis mean at time k

$$[\bar{\mathbf{x}}_k^a]^j = [\bar{\mathbf{x}}_{fk}]^j + \frac{\alpha_j}{\alpha_j + r} ([y_k]^j - [\bar{\mathbf{x}}_{fk}]^j). \quad (43)$$

The j^{th} diagonal element of the posterior covariance becomes

$$[\mathbf{P}_\infty^a]^{jj} = \alpha_j - \frac{(\alpha_j)^2}{\alpha_j + r} = \frac{\alpha_j r}{\alpha_j + r}. \quad (44)$$

3.2.2 Diffusion DA

Here we will extend the typical training paradigm of diffusion modeling to the Bayesian posterior distribution with a cycling prior, i.e., the posterior distribution typically targeted in conventional DA. As explained before, the “training set” for ML is typically taken to be the climatological prior, but in the simplified problem setup we are working in, one can imagine a diffusion DA system that re-trains at every cycle (see [Bao et al. \(2024\)](#) for another example).

The procedure is as follows.

1. Initially, we build a diffusion model as in Section 3.3.1.3.1.2 for the pdf $p(\mathbf{x}_0|\mathbf{y}_0)$.
2. We use this diffusion model to generate a large training set consistent with $p(\mathbf{x}_0|\mathbf{y}_0)$.
3. We use the forecast model (17) to push each member of this set forward to the time of the next set of observations, \mathbf{y}_1 .
4. We then use these forecasts as the training set to build a new diffusion model that produces samples from $p(\mathbf{x}_1|\mathbf{y}_1, \mathbf{y}_0)$.
5. We then repeat steps 3 and 4 for each cycle k for which we desire to process observations.

We imagine we have done this up to the k^{th} cycle and that the covariances have converged to their steady-state values. In this case, the typical diffusion model loss function would be modified to draw its training set from the k^{th} cycling *joint* posterior, i.e.,

$$p(\mathbf{x}_k, \mathbf{y}_k | \mathbf{y}_{k-1}, \mathbf{y}_{k-2}, \dots) = p(\mathbf{y}_k | \mathbf{x}_k) p(\mathbf{x}_k | \mathbf{y}_{k-1}, \mathbf{y}_{k-2}, \dots) \quad (45)$$

where we emphasize that $p(\mathbf{x}_k | \mathbf{y}_{k-1}, \mathbf{y}_{k-2}, \dots)$ is the cycling prior and $p(\mathbf{y}_k | \mathbf{x}_k)$ is the standard Gaussian observation likelihood. This implies the following loss

$$\ell = E_{\mathbf{x}_k, \mathbf{y}_k \sim p(\mathbf{x}_k, \mathbf{y}_k | \mathbf{y}_{k-1}, \mathbf{y}_{k-2}, \dots)} E_{n \sim \mathcal{N}(0, t^2)} \|\mathbf{x}_k - \mathbf{D}(\mathbf{v} = \mathbf{x}_k + n, \mathbf{y}_k, t)\|_2^2, \quad (46)$$

Note that this loss function implies that we re-train the diffusion model at each and every cycle.

In any event, the minimum of this loss function for this linear, Gaussian system is simply

$$\mathbf{D}(\mathbf{v}, \mathbf{y}_k; t) = E_{\mathbf{x}_k \sim p(\mathbf{x}_k | \mathbf{y}_k, \mathbf{y}_{k-1}, \dots)} [\mathbf{x}_k] = \bar{\mathbf{x}}_{fk} + \mathbf{P}_\infty^f \hat{\mathbf{H}}^T [\hat{\mathbf{H}} \mathbf{P}_\infty^f \hat{\mathbf{H}}^T + \mathbf{R}]^{-1} \hat{\mathbf{y}} \quad (47)$$

where

$$\mathbf{R} = \begin{bmatrix} t^2 \mathbf{I}_{n_x} & \mathbf{0} \\ \mathbf{0} & r \mathbf{I}_{n_o} \end{bmatrix}, \quad \hat{\mathbf{y}} = \begin{bmatrix} \mathbf{v} - \bar{\mathbf{x}}_{fk} \\ \mathbf{y} - \mathbf{H} \bar{\mathbf{x}}_{fk} \end{bmatrix}. \quad (48)$$

We then apply Tweedie's formula to find the following SDE:

$$d\mathbf{v} = -\frac{2}{t} \left[\mathbf{P}_\infty^f \hat{\mathbf{H}}^T [\hat{\mathbf{H}} \mathbf{P}_\infty^f \hat{\mathbf{H}}^T + \mathbf{R}]^{-1} \hat{\mathbf{y}} - (\mathbf{v} - \bar{\mathbf{x}}_{fk}) \right] dt + \sqrt{2t} d\bar{\beta}_t, \quad (49)$$

As we did in the previous sections we consider the j^{th} observed grid point. In this case, the reverse process can be written as

$$dv = -\frac{2}{t} \left[\frac{\frac{\alpha^j r}{\alpha^j + r}}{\frac{\alpha^j r}{\alpha^j + r} + t^2} (v - \bar{x}) + \frac{\frac{\alpha^j t^2}{\alpha^j + r}}{\frac{\alpha^j r}{\alpha^j + r} + t^2} (y - \bar{x}) - (v - \bar{x}) \right] dt + \sqrt{2t} d\bar{\beta}_t \quad (50)$$

where $y = [\mathbf{y}_k]^j$ and $\bar{x} = [\bar{\mathbf{x}}_{fk}]^j$. We can solve this SDE analytically (see Appendix C):

$$\begin{aligned} v(0) = & \bar{x} + \frac{\frac{\alpha^j r}{\alpha^j + r}}{\frac{\alpha^j r}{\alpha^j + r} + T^2} (v(T) - \bar{x}) + \frac{(\alpha^j)^2 r}{(\alpha^j + r)^2} \frac{T^2}{\frac{\alpha^j r}{\alpha^j + r} (\frac{\alpha^j r}{\alpha^j + r} + T^2)} ([\mathbf{y}_k]^j - \bar{x}) \\ & + \frac{\alpha^j r}{\alpha^j + r} \int_T^0 \frac{\sqrt{2t}}{\frac{\alpha^j r}{\alpha^j + r} + t^2} d\bar{\beta}_t, \end{aligned} \quad (51)$$

We first compute the mean:

$$\langle v(0) \rangle = \bar{x} + \frac{\frac{\alpha^j r}{\alpha^j + r}}{\frac{\alpha^j r}{\alpha^j + r} + T^2} (\langle v(T) \rangle - \bar{x}) + \frac{(\alpha^j)^2 r}{(\alpha^j + r)^2} \frac{T^2}{\frac{\alpha^j r}{\alpha^j + r} (\frac{\alpha^j r}{\alpha^j + r} + T^2)} y. \quad (52)$$

In the limit as $T \rightarrow \infty$ the mean simplifies to

$$\langle v(0) \rangle_{T \rightarrow \infty} = \bar{x} + \frac{\alpha^j}{\alpha^j + r} (y - \bar{x}) \quad (53)$$

which is equal to the cycling posterior mean derived via the Kalman filter in (43).

Second, we find the variance,

$$\langle (v(0) - \langle v(0) \rangle)^2 \rangle = \frac{\frac{\alpha^j r}{\alpha^j + r}}{\frac{\alpha^j r}{\alpha^j + r} + T^2} \langle (v(T) - \langle v(T) \rangle)^2 \rangle + \left\langle \left(\frac{\alpha^j r}{\alpha^j + r} \int_T^0 \frac{\sqrt{2t}}{\frac{\alpha^j r}{\alpha^j + r} + t^2} d\bar{\beta}_t \right)^2 \right\rangle \quad (54)$$

where we have used the fact that the cross-term vanishes. The stochastic integral on the right-hand side requires the use of the Itô isometry, i.e.,

$$\begin{aligned} \left\langle \left(\int_T^0 \frac{\sqrt{2t}}{\frac{\alpha^j r}{\alpha^j + r} + t^2} d\bar{\beta}_t \right)^2 \right\rangle &= \left\langle \left(- \int_0^T \frac{\sqrt{2t}}{\frac{\alpha^j r}{\alpha^j + r} + t^2} d\bar{\beta}_t \right)^2 \right\rangle \\ &= 2 \int_0^T \frac{t}{(\frac{\alpha^j r}{\alpha^j + r} + t^2)^2} dt = -2 \int_T^0 \frac{t}{(\frac{\alpha^j r}{\alpha^j + r} + t^2)^2} dt \end{aligned} \quad (55)$$

Thus, the variance becomes

$$\langle (v(0) - \langle v(0) \rangle)^2 \rangle = \frac{(\alpha^j)^2 r^2 T^2}{(\alpha^j + r)^2} + \frac{\alpha^j r}{\alpha^j + r} \frac{T^2}{\alpha^j + r + T^2}. \quad (56)$$

In the limit as $T \rightarrow \infty$ the variance is

$$\langle (v(0) - \langle v(0) \rangle)^2 \rangle_{T \rightarrow \infty} = \frac{\alpha^j r}{\alpha^j + r} \quad (57)$$

which is the posterior variance we obtained via the Kalman filter in (44). We have thus shown that retraining a diffusion model at each DA cycle, using the latest prior, results in a diffusion DA system that samples the same posterior pdf as a conventional ensemble DA system that uses a cycling prior.

3.3 DA with an extended likelihood

We now consider DA systems that ingest the observations as well as a forecast, but treat this forecast essentially as an additional observation. We will denote the forecast at time k by \mathbf{f}_k and assume that it is derived from a single model forecast from the posterior mean at time $k - 1$. In this way we will bring information from the past into the latest state estimate.

If we assume the usual observation equation (18), we have that $p(\mathbf{y}_k | \mathbf{x}_k, \mathbf{f}_k) = p(\mathbf{y}_k | \mathbf{x}_k)$ so that (15) becomes

$$p(\mathbf{x}_k | \mathbf{y}_k, \mathbf{f}_k) \propto p(\mathbf{y}_k | \mathbf{x}_k) p(\mathbf{f}_k | \mathbf{x}_k) p(\mathbf{x}_k). \quad (58)$$

Here, $p(\mathbf{x}_k)$ is the climatological prior, $p(\mathbf{y}_k | \mathbf{x}_k)$ is the usual Gaussian observation likelihood and $p(\mathbf{f}_k | \mathbf{x}_k)$ is the extension of the likelihood to include the forecast \mathbf{f}_k .

While it is clear what the climatological prior and Gaussian observation likelihood are, at first blush it is far less clear what the forecast likelihood is. Note however that in this linear, Gaussian system the posterior mean at time $k - 1$ is a linear function of the observation (see equation (23)), which, because the observation is a linear function of the truth (see equation (18)), implies that the forecast is also a linear function of the truth. Furthermore, for the example problem of this section, the Kalman gain is a number less than one and the observation is multiplied by this Kalman gain (again see equation (23)). Hence, there will be a linear relation between the forecast \mathbf{f}_k and the “truth” \mathbf{x}_k of the form

$$\mathbf{f}_k = a \mathbf{x}_k + \boldsymbol{\varepsilon}_f, \quad \boldsymbol{\varepsilon}_f \sim \mathcal{N}(\mathbf{0}, r_f \mathbf{I}), \quad (59)$$

where $a \leq 1$ and r_f are scalars. Note that r_f denotes the error variance of the forecast and a is determined from the steady-state Kalman gain, \mathbf{K}_∞ , and the drift term in (17). In the numerical illustration below we will carefully discuss how we determined the scalars a and r_f . Finally, we emphasize that this form for $p(\mathbf{f}_k | \mathbf{x}_k)$ is entirely dependent on the linear, Gaussian nature of (17). Consequently, in a nonlinear problem the structure of (59) would generally require a nonlinear function of \mathbf{x}_k and a non-Gaussian error distribution. This would be very difficult to determine explicitly in a typical geophysical system, but could be learned implicitly within a diffusion model.

3.3.1 Bayesian posterior

As before, we first use the Kalman filter formalism. Since the forecast is treated as an additional observation, we simply find a Kalman filter of the following form

$$\bar{\mathbf{x}}_a = \mathbf{H}_e^T [\mathbf{H}_e \mathbf{H}_e^T + \mathbf{R}_e]^{-1} \mathbf{y}_e \quad (60)$$

but with an extended observation and observation error covariance matrix, viz.

$$\mathbf{y}_e = \begin{bmatrix} \mathbf{y}_k \\ \mathbf{f}_k \end{bmatrix}, \quad \mathbf{H}_e = \begin{pmatrix} \mathbf{H} \\ a\mathbf{I} \end{pmatrix}, \quad \mathbf{R}_e = \begin{pmatrix} r\mathbf{I} & \mathbf{0} \\ \mathbf{0} & r_f\mathbf{I} \end{pmatrix}. \quad (61)$$

Repeating the same calculation as in Section 3.1.1 gives the elements of the posterior mean and posterior variance:

$$[\mathbf{x}_k^a]^j = \frac{1}{1 + r + a^2 \frac{r}{r_f}} \left(y + a \frac{r}{r_f} f \right), \quad (62)$$

$$[\mathbf{P}^a]^{jj} = \frac{r}{1 + r + a^2 \frac{r}{r_f}}. \quad (63)$$

where $[\mathbf{f}_k]^j = f$. We note that as $r_f \rightarrow \infty$, that this posterior disregards the forecast and we recover the results from Section 3.3.1.3.1.1 as expected.

3.3.2 Diffusion DA

In this case, the typical diffusion model loss function would be modified to draw its training set from the extended *joint* posterior, i.e. ,

$$p(\mathbf{x}_k, \mathbf{y}_k, \mathbf{f}_k) = p(\mathbf{y}_k | \mathbf{x}_k) p(\mathbf{f}_k | \mathbf{x}_k) p(\mathbf{x}_k) \quad (64)$$

where we emphasize that the prior here is the climatological one. This implies the following loss

$$\ell = E_{\mathbf{x}_k, \mathbf{y}_k, \mathbf{f}_k \sim p(\mathbf{x}_k, \mathbf{y}_k, \mathbf{f}_k)} E_{n \sim \mathcal{N}(0, t^2)} \|\mathbf{x}_k - \mathbf{D}(\mathbf{v} = \mathbf{x}_k + n, t, \mathbf{y}_k, \mathbf{f}_k)\|_2^2, \quad (65)$$

The minimum of (65) for a linear, Gaussian problem is as before a kind of Kalman filter of the form

$$\mathbf{D}(\mathbf{v}, t, \mathbf{y}_k, \mathbf{f}_k) = E_{\mathbf{x}_k \sim p(\mathbf{x}_k | \mathbf{v}, \mathbf{y}_k, \mathbf{f}_k)} [\mathbf{x}_k] = \hat{\mathbf{H}}^T [\hat{\mathbf{H}} \hat{\mathbf{H}}^T + \mathbf{R}]^{-1} \hat{\mathbf{y}} \quad (66)$$

where

$$\mathbf{R} = \begin{bmatrix} t^2 \mathbf{I}_{n_x} & \mathbf{0}_{n_x \times n_o} & \mathbf{0}_{n_x} \\ \mathbf{0}_{n_o \times n_x} & r \mathbf{I}_{n_o} & \mathbf{0}_{n_o \times n_x} \\ \mathbf{0}_{n_x} & \mathbf{0}_{n_x \times n_o} & r_f \mathbf{I} \end{bmatrix}, \quad \hat{\mathbf{H}} = \begin{bmatrix} \mathbf{I}_{n_x} \\ \mathbf{H} \\ a \mathbf{I}_{n_x} \end{bmatrix}, \quad \hat{\mathbf{y}} = \begin{bmatrix} \mathbf{v} \\ \mathbf{y}_k \\ \mathbf{f}_k \end{bmatrix}. \quad (67)$$

We then use this denoiser to determine the associated diffusion model, viz.

$$d\mathbf{v} = -\frac{2}{t} \left[\hat{\mathbf{H}}^T [\hat{\mathbf{H}} \hat{\mathbf{H}}^T + \mathbf{R}]^{-1} \hat{\mathbf{y}} - \mathbf{v} \right] dt + \sqrt{2t} d\bar{\beta}_t \quad (68)$$

Upon repeating the same steps in Section 3.3.1.3.1.2 we find that the mean of the observed variable is

$$\langle v(0) \rangle = \frac{\gamma}{\gamma + T^2} \langle v(T) \rangle + \frac{\gamma}{r} \frac{T^2}{\gamma + T^2} y + a \frac{\gamma}{r_f} \frac{T^2}{\gamma + T^2} f, \quad (69)$$

where we introduced

$$\gamma = \frac{r}{1 + r + a^2 \frac{r}{r_f}}, \quad (70)$$

as a shorthand notation for the posterior variance. For $T \rightarrow \infty$ we obtain

$$\lim_{T \rightarrow \infty} \langle v(0) \rangle = \frac{\gamma}{r} y + a \frac{\gamma}{r_f} f, \quad (71)$$

which upon rearrangement is the same as the Bayesian posterior result in (62). Similarly, we find the variance of an observed quantity to be

$$\langle (v(0) - \langle v(0) \rangle)^2 \rangle = \frac{\gamma^2 T^2}{(\gamma + T^2)^2} + \gamma \frac{T^2}{\gamma + T^2}, \quad (72)$$

which, for $T \rightarrow \infty$ is equal to γ which is the variance computed via the Kalman formalism in (63).

Hence, we have now shown that a diffusion model that is trained on a long time-series of system states of a dynamical system along with observations and forecasts of that dynamical system results in a diffusion DA system that samples a Bayesian posterior distribution constructed with an extended likelihood, and, possibly more importantly, all the while using the climatological prior.

4 Numerical illustration

We illustrate the various forms of Bayes' rule and their corresponding diffusion models of Section 3 with a specific example.

4.1 Discretization of the dynamical model

We solve the SDE in (17) numerically using the forward Euler method, i.e.,

$$\mathbf{x}_{k+1} = D\mathbf{x}_k + \sqrt{\Delta}\mathbf{w}_k, \quad (73)$$

where Δ is the time step, \mathbf{w}_k is a random draw from $N(\mathbf{0}, \mathbf{I}_{n_x})$, the state vector, \mathbf{x}_k , is of length $n_x = 100$, and

$$D = 1 - \frac{\Delta}{2}. \quad (74)$$

Because we are working with a linear, Gaussian system and a linear observation operator, the optimal DA system is the Kalman filter. That is, we can propagate the mean and covariance matrix forward in time without recourse to an ensemble, i.e.,

$$\bar{\mathbf{x}}_{k+1} = D\bar{\mathbf{x}}_k, \quad (75)$$

$$\mathbf{P}_{k+1}^f = D^2\mathbf{P}_k^f + \Delta\mathbf{I}_{n_x}. \quad (76)$$

Because our forward Euler (FE) discretization is accurate to first-order in Δ , equation (76) converges at large time to

$$\mathbf{P}_c^f = \frac{4}{4 - \Delta}\mathbf{I} \quad (77)$$

rather than $\mathbf{P}_c = \mathbf{I}$ as expected from our continuous time analysis (see Equation (20)). We will use this discrete time climatological covariance to ensure consistency in the experiments described below.

4.2 Data assimilation

4.2.1 Kalman filtering

The Kalman filter with a climatological prior evaluates the equation for the posterior mean (23) at each cycle. The Kalman filter with a cycling prior (Section 3.3.2.3.2.1) is initialized with the climatological moments of $\mathbf{P}_0 = \mathbf{P}_c$ and $\bar{\mathbf{x}}_0 = \mathbf{0}$. The discrete model is used to propagate the

posterior mean and covariance (see equations (75) and (76)) forward in time to the next set of observations. The Kalman filter with an extended likelihood uses the posterior mean and covariance equations in Section 3.3.3.3.1. Moreover, at each cycle we use the discretized model (equation (73)) to integrate the posterior mean forward in time to the next cycle.

Finally, we must specify the parameters a and r_f for the Kalman filter with an extended likelihood. We leverage the following strategy with the ultimate goal of finding a combination of a and r_f such that the posterior mean squared error (MSE) of the Kalman filter matches its posterior variance prediction, which is key to verifying that the theory is matching the experiment. We initialize the process with $a = 1$ and $r_f = 1$ and cycle the corresponding Kalman filter for 10^5 times to collect truth and forecast pairs $([\mathbf{x}_k]^j, [\mathbf{f}_k]^j)$ at each grid point j . We then fit two functions to this large dataset of forecast-truth pairs. First, we can fit a line through the data because the mean of $p(\mathbf{f}_k|\mathbf{x}_k)$ is $a\mathbf{x}_k$, so that the slope of the line can be used as a candidate value for a . Second, we can compute the MSE associated with the *forecast*, i.e.,

$$\text{MSE}_f = E [([\mathbf{f}_k]_j - [\mathbf{x}_k]_j)^2] = (1 - a)^2 [\mathbf{x}_k]_j^2 + r_f, \quad (78)$$

and subsequently fit a quadratic to obtain another estimate of the parameter a and also an estimate of the parameter r_f . We then repeat this process by re-running the cycling experiment with the new values of a and r_f until the two estimates of a agree to two decimal places. As an example, for the case of $\Delta = 0.1$, the system settled on $a = 0.61$ and $r_f = 0.34$ and the time-averaged MSE of the Kalman filter was then very close to the posterior variance prediction. We realize that this strategy is likely to not be practical in typical geophysical systems. The goal here is as a benchmark to the associated diffusion model and not as a practical algorithm.

4.2.2 Diffusion models

We build a diffusion model using a cycling prior of the form (49) using a simple FE-based method, viz.

$$\mathbf{v}_{n-1} = \mathbf{v}_n - \frac{2}{t_n} \left[\mathbf{P}_i^f \hat{\mathbf{H}}^T [\hat{\mathbf{H}} \mathbf{P}_i^f \hat{\mathbf{H}}^T + \mathbf{R}]^{-1} \hat{\mathbf{y}} - (\mathbf{v}_n - \bar{\mathbf{x}}_i) \right] \Delta_d + \sqrt{2t_n |\Delta_d|} \mathbf{w}_n \quad (79)$$

where

$$\hat{\mathbf{y}} = \begin{bmatrix} \mathbf{v} - \bar{\mathbf{x}}_i \\ \mathbf{y}_k - \mathbf{H} \bar{\mathbf{x}}_i \end{bmatrix} \quad (80)$$

with $\hat{\mathbf{H}}$ and \mathbf{R} being defined as in section 3.2.2 and we generate the i^{th} sample as $\mathbf{x}^{(i)} = \mathbf{v}_0$. We use 1000 internal virtual time steps denoted by the subscript, n , for the reverse integration with a time step of $\Delta_d = -0.1$ and we repeat this to create an ensemble of $n_e = 10^4$ members. Because the reverse process must start from a large virtual time we integrate this equation starting at an arbitrarily chosen time of $T = 100$ back to $t = 0$ on a uniform temporal grid. From these ensemble members we then calculate a posterior ensemble mean and covariance matrix. Lastly, we then propagate this posterior ensemble mean and covariance matrix forward to the next set of observations using (75) and (76).

For the climatological diffusion model we also solve (31) using a simple FE-based method, viz.

$$\mathbf{v}_{n-1} = \mathbf{v}_n - \frac{2}{t_n} \left[\mathbf{P}_c^f \hat{\mathbf{H}}^T [\hat{\mathbf{H}} \mathbf{P}_c^f \hat{\mathbf{H}}^T + \mathbf{R}]^{-1} \hat{\mathbf{y}} - \mathbf{v}_n \right] \Delta_d + \sqrt{2t_n |\Delta_d|} \mathbf{w}_n \quad (81)$$

where

$$\hat{\mathbf{y}} = \begin{bmatrix} \mathbf{v} \\ \mathbf{y}_k \end{bmatrix} \quad (82)$$

with $\hat{\mathbf{H}}$ and \mathbf{R} being defined as in section 3.1.2. We again create $n_e = 10^4$ members from which we determine the posterior ensemble mean and covariance that we report below. In distinction to the diffusion model with the cycling prior these posterior ensemble mean and covariances are not used in any way at the next cycle.

For the extended likelihood diffusion model we solve (68) using a FE method as

$$\mathbf{v}_{n-1} = \mathbf{v}_n - \frac{2}{t_n} \left[\mathbf{P}_c^f \hat{\mathbf{H}}^T [\hat{\mathbf{H}} \mathbf{P}_c^f \hat{\mathbf{H}}^T + \mathbf{R}]^{-1} \hat{\mathbf{y}} - \mathbf{v}_n \right] \Delta_d + \sqrt{2t_n |\Delta_d|} \mathbf{w}_n \quad (83)$$

where

$$\hat{\mathbf{y}} = \begin{bmatrix} \mathbf{v} \\ \mathbf{y}_k \\ \mathbf{f}_k \end{bmatrix} \quad (84)$$

with $\hat{\mathbf{H}}$ and \mathbf{R} being defined as in section 3.3.2. These matrices require knowledge of a and r_f , for which we use the same values determined using the Kalman filter setup. Similar to the diffusion model using the climatological prior we create $n_e = 10^4$ members from which we determine the posterior ensemble mean and covariance. However, in distinction to the diffusion model using the climatological prior we now take the posterior mean and integrate it forward in time to the next set of observations using (73) to obtain the forecast, \mathbf{f}_k .

4.2.3 Results

We first run an experiment with $\Delta = 0.1$ in which we observe every state element ($\mathbf{H} = \mathbf{I}$) and collect observations at every time step of the model; the observation error variance is $r = 1$. This experiment, and the others reported below, will use a set of $n_y = 100$ observations. The posterior MSE and posterior variance are summarized in Figure 1, for three DA setups (climatological prior, extended likelihood and cycling prior), solved analytically via the corresponding Kalman formalisms, or via a diffusion model. As expected from our theory, we observe that (i) the diffusion models successfully emulate the corresponding Kalman methods, i.e., the diffusion models emulate their associated form of Bayes' rule; (ii) a DA system with a cycling prior generates the smallest MSE and posterior variance, while DA systems with a climatological prior or an extended likelihood lead to larger errors; (iii) bringing in a forecast via an extended likelihood improves the state estimates when compared to a DA system with a climatological prior, but the errors and variances are still larger than what a fully cycled DA system can achieve.

This example provides a numerical confirmation of our theory. In particular, this example shows that the various forms of Bayes' rule being described by the Kalman filters are in fact realized by the particular choices used to construct the training sets used to create the three diffusion models. The posterior using climatological prior realized via a Kalman filter or diffusion model produce the same moments for the posterior and, hence, the two systems are indeed working with the same form of Bayes' rule. Analogous results hold for the posteriors defined by a cycling prior or an extended likelihood. It is also important to check that the posterior variance correctly matches the time-averaged MSE for all methods, which is the most important indicator that the theory is working correctly.

Intuitively, as the time interval between observations, Δ , becomes larger, past observations carry less information and thus one would expect that the cycling prior converges to the climatological prior as Δ becomes large. We now test this and other notions in numerical experiments in which we vary Δ and the observation error variance, r , and then compare the steady-state posterior

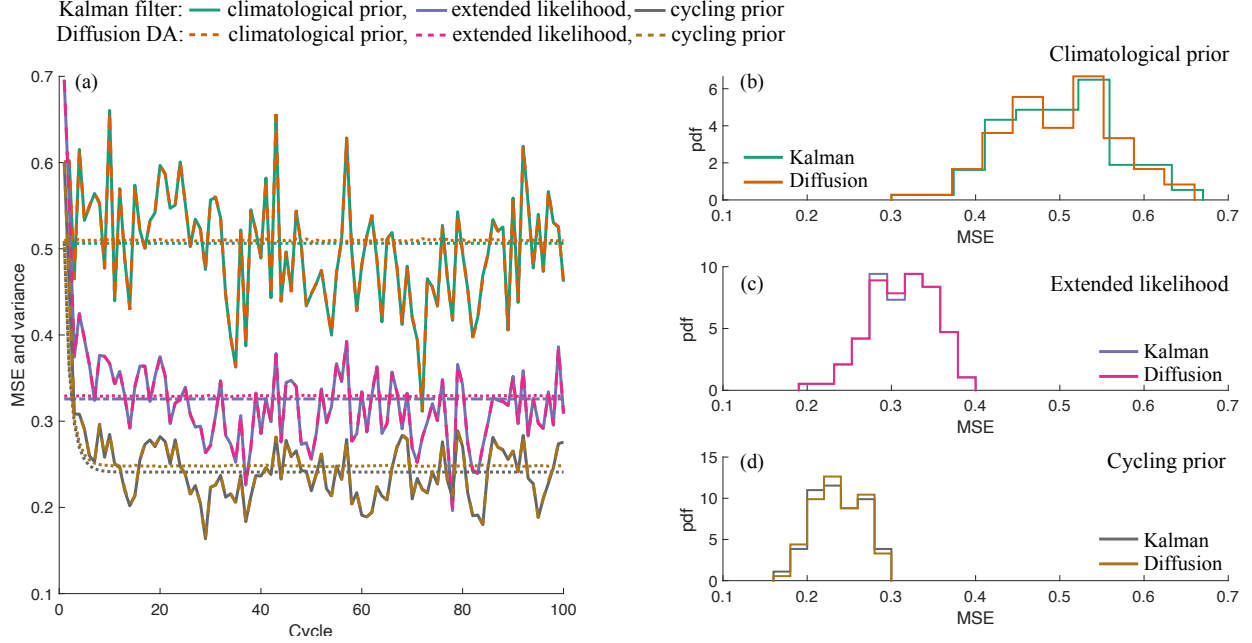


Figure 1: (a) MSE (solid or dashed) and variance (dotted) for three different Bayesian posterior distributions, corresponding to a climatological prior, a cycling prior and an extended likelihood. Shown are results obtained with Kalman filters (analytical solutions, solid) and diffusion models (dashed). Note that the MSE curves for the Kalman filter methods coincide with those of the diffusion models, indicating that the two methods produce identical results. The posterior variances are slightly different between the Kalman and diffusion-based methods because of small errors due to the choice of the FE method for the solution of the diffusion models' SDEs. (b)-(d) Histograms of the MSE after a 20-cycle spin-up period. Again, the diffusion models produce nearly identical results as the Kalman filter methods, and we see that MSE decreases (on average and in distribution) when moving from a DA system with a climatological prior, to one with an extended likelihood, to one with a cycling prior.

covariance of a DA system with a cycling prior to that of a DA system with a climatological prior. To this end, we repeat these cycling DA experiments for various observation error variances (r) and summarize our results in Figure 2(a). Note that as the time between observations increases from $\Delta = 0.01$ to $\Delta = 2$, the posterior variance using the cycling prior indeed converges to the posterior variance using the climatological prior. Hence, the time between observations strongly controls the difference between those two forms of Bayes' rule and the resulting DA systems. More specifically, there is a delicate balance between the timescale of the error growth induced by the stochastic term in (17) and the variance reducing property of the assimilation of observations. If the error growth dominates (large time interval between observations), DA systems with a cycling prior are nearly identical to DA systems with a climatological prior. If the assimilation of observations is frequent (short time interval between observations), then the cycling prior propagates information from past DA cycles to the current ones and, therefore, reduces state estimation errors and posterior variances.

Finally, we perform a set of experiments in which we vary the observation error variance for the DA system with an extended likelihood. We keep the time interval between observations fixed (at $\Delta = 0.1$) because for each value of r we need to tune the parameters a and r_f of the extended

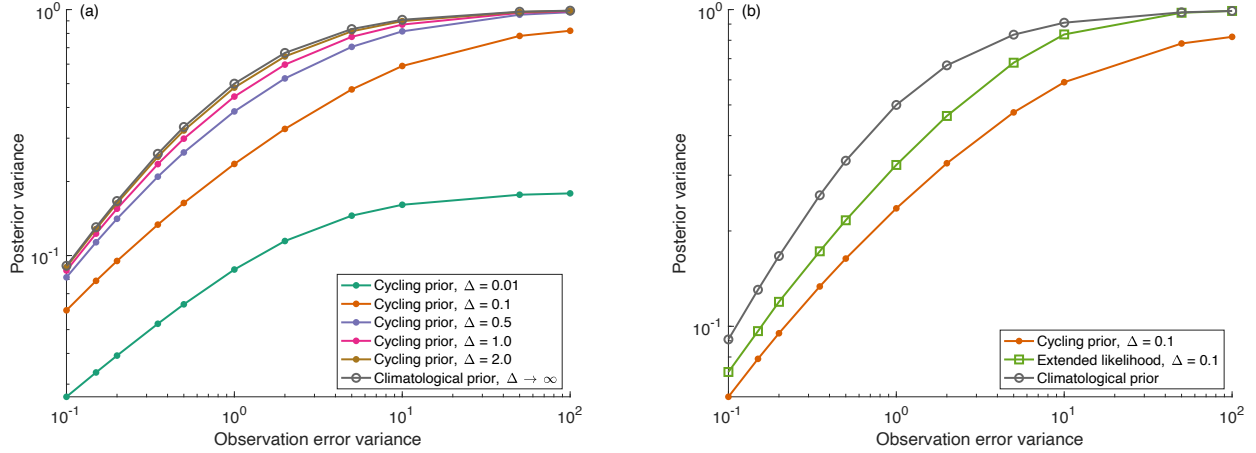


Figure 2: (a) Steady state posterior variance of a DA system with a cycling prior as a function of observation error and time interval between observations. Also shown is the steady state posterior variance of a DA system with a climatological prior, which corresponds to a very large timer interval between observations. (b) Steady state posterior variance of a DA system with an extended likelihood as a function of observation error (time interval between observations is $\Delta = 0.1$). Also shown are the posterior variances of a DA system with a cycling prior and with a climatological prior.

likelihood system. Results are summarized in Figure 2(b), where we show the posterior variance of an extended likelihood DA system as a function of the observation error variance. For comparison, we also plot the posterior variance of a DA system with a climatological prior and with a cycling prior (already shown in Figure 2(b)).

We note that the posterior variance of a DA system with an extended likelihood is in between that of a system with a cycling or climatological prior, unless r is very large (see below). Thus, for moderate r , the extended likelihood indeed propagates information from previous assimilation steps via a single forecast. The posterior variance of the extended likelihood DA system, however, is larger than that of a DA system with a cycling prior, which indicates that more information is transmitted between cycles when the entire distribution is propagated, rather than a single forecast. Moreover, the posterior variance of a DA system with an extended likelihood converges to the posterior variance of a DA system with a climatological prior as the observation error variance r becomes large. This is due to the fact that the information from the forecast is only as good as the information in the posterior mean it is integrated from. As the observation error increases we find that r_f also increases such that there is less information in the forecast and therefore the differences between the posterior using a climatological prior and the posterior using the extended likelihood become muted. Note, however, that there is still a large difference between the posterior variance using a cycling prior and the posterior variance using the climatological prior even for very large observation error variances. Hence, we again see that propagating the entire distribution leads to more accurate state estimates than propagating a single forecast.

5 Summary and conclusions

We have shown that a diffusion DA system can target different Bayesian posterior distributions and we have explored, in detail, three versions: a Bayesian posterior with a cycled prior, which is typical of conventional DA systems (equation (1)), a Bayesian posterior with a climatological prior (equation (14)), and a Bayesian posterior in which the likelihood is extended with a single forecast (equation (58)) that is treated like an additional predictor. We have shown three different ways to construct training sets that lead to diffusion models that sample each of these three Bayesian posterior distributions.

The key aspect of the differences between these versions of Bayes’ rule is in their use of the prior. In both the posterior using a climatological prior and the posterior using an extended likelihood the training set is determined from a long time-series of past weather. This long time-series of past weather constitutes random samples from a climatological prior. This climatological prior is never updated in these versions of the posterior. Hence, both these systems ostensibly require only a single training. However, we envision two possible ways one might make use of the posterior using an extended likelihood. In the first way, one might run the extended likelihood diffusion model alongside a conventional DA system. This conventional DA system would produce the forecast used in the extended likelihood diffusion model. Because the quality of the forecast from the conventional DA system is stationary the training set will correctly provide the appropriate examples. However, the second way one might make use of the posterior using an extended likelihood is with a self-sufficient diffusion model that produces its own forecasts. We speculate that the iterative procedure we used to find a and r_f implies that using the posterior with an extended likelihood in a diffusion model will require multiple training attempts to get the forecasts produced from the diffusion-based DA system to be of the same quality as the ones trained upon. Therefore, in this second case the posterior using the extended likelihood is likely to be more computationally demanding in order to obtain a near optimal system. Of course, one could ignore this warning and simply train this extended likelihood diffusion model once, but in our experiments (not shown) we found this to lead to a system that produced ensembles whose variance was not as carefully calibrated to the MSE of the ensemble mean. Furthermore, the posterior using a cycled prior quite obviously updates its prior training set at each and every cycle. This requires re-training of the diffusion model at every cycle, and is therefore the most computationally demanding system we examined. Given the number of samples required to train typical diffusion model architectures this implies a significant expense in both the generation of the new training set as well as in the training itself.

Nevertheless, the posterior using a cycled prior had nearly universally lower errors than the other two posterior distributions. Only when the observations were so far apart in time that the observations entirely de-correlated did all three versions of Bayes’ rule deliver a similar answer. Hence, we suggest that future research should be directed towards ways in which we can make use of the posterior with a cycling prior in the most efficient ways possible. For example, it may be that the difference between the diffusion model at cycle $k - 1$ and k is small enough that one could make use of fine-tuning methods (see e.g. [Parthasarathy et al. \(2024\)](#)) and/or transfer learning (see e.g. [Zhuang et al. \(2020\)](#)). Similarly, future research into variations on the likelihood based approximations in [Chung et al. \(2023\)](#) as applied to the posteriors for the extended likelihood and cycling prior may also lead to ways in which we can accelerate the training required. Work in these directions is already underway.

Acknowledgments

DH is supported by the US Office of Naval Research (ONR) grant N0001422WX00451. MM is supported by the US ONR grant N000142512298.

Data Statement

The code used for making the figures will be made available on github.

Appendices

A Tweedie's formula

For Tweedie's formula, we consider a random variable v , conditioned on a random variable x , such that

$$v|x = x + \varepsilon, \quad \varepsilon \sim \mathcal{N}(0, \sigma_0^2), \quad (85)$$

which implies the conditional pdf

$$p(v|x) = \frac{1}{\sqrt{2\pi}\sigma_0} \exp\left(-\frac{1}{2}\left(\frac{v-x}{\sigma_0}\right)^2\right). \quad (86)$$

We wish to compute

$$\frac{d}{dv} \log p(v) = \frac{1}{p(v)} \frac{d}{dv} p(v). \quad (87)$$

Using the fact that

$$p(v) = \int_{-\infty}^{\infty} p(v|x)p(x)dx, \quad (88)$$

we find

$$\frac{d}{dv} p(v) = \int_{-\infty}^{\infty} \frac{x-v}{\sigma_0^2} p(v|x)p(x)dx. \quad (89)$$

Thus

$$\frac{d}{dv} \log p(v) = \int_{-\infty}^{\infty} \frac{x-v}{\sigma_0^2} \frac{p(v|x)p(x)}{p(v)} dx, \quad (90)$$

which simplifies to

$$\frac{d}{dv} \log p(v) = \int_{-\infty}^{\infty} \frac{x-v}{\sigma_0^2} p(x|v) dx, \quad (91)$$

since

$$\frac{p(v|x)p(x)}{p(v)} = \frac{\frac{p(v,x)}{p(x)}p(x)}{p(v)} = \frac{p(v,x)}{p(v)} = p(x|v). \quad (92)$$

Distributing the integral leads to

$$\frac{d}{dv} \log p(v) = \frac{1}{\sigma_0^2} \int_{-\infty}^{\infty} xp(x|v)dx - v \int_{-\infty}^{\infty} p(x|v)dx = \frac{1}{\sigma_0^2} (E[x|v] - v), \quad (93)$$

which, upon rearrangement, gives Tweedie's formula:

$$E[x|v] = v + \sigma_0^2 \frac{d}{dv} \log(p(v)). \quad (94)$$

B Solution to the SDE in (32)

We begin with (32) and perform a few simple manipulations:

$$dv = -\frac{2}{t} \left[\frac{\frac{r}{1+r}}{\frac{r}{1+r} + t^2} v + \frac{\frac{t^2}{1+r}}{\frac{r}{1+r} + t^2} y - v \right] dt + \sqrt{2t} d\bar{\beta}_t, \quad (95)$$

$$dv = -\frac{2}{t} \left[-\frac{t^2}{\frac{r}{1+r} + t^2} v + \frac{\frac{t^2}{1+r}}{\frac{r}{1+r} + t^2} y \right] dt + \sqrt{2t} d\bar{\beta}_t, \quad (96)$$

$$dv - 2t \frac{1}{\frac{r}{1+r} + t^2} v dt = -2t \frac{\frac{1}{1+r}}{\frac{r}{1+r} + t^2} y dt + \sqrt{2t} d\bar{\beta}_t, \quad (97)$$

$$\frac{1}{\frac{r}{1+r} + t^2} dv - 2t \frac{1}{(\frac{r}{1+r} + t^2)^2} v dt = -2t \frac{\frac{1}{1+r}}{(\frac{r}{1+r} + t^2)^2} y dt + \frac{\sqrt{2t}}{\frac{r}{1+r} + t^2} d\bar{\beta}_t. \quad (98)$$

$$d\left(\frac{1}{\frac{r}{1+r} + t^2} v\right) = -2t \frac{\frac{1}{1+r}}{(\frac{r}{1+r} + t^2)^2} y dt + \frac{\sqrt{2t}}{\frac{r}{1+r} + t^2} d\bar{\beta}_t. \quad (99)$$

Integrating backwards in time, from T to 0,

$$\int_T^0 d\left(\frac{1}{\frac{r}{1+r} + t^2} v(t)\right) = -2y \int_T^0 \frac{\frac{1}{1+r} t}{(\frac{r}{1+r} + t^2)^2} dt + \int_T^0 \frac{\sqrt{2t}}{\frac{r}{1+r} + t^2} d\bar{\beta}_t, \quad (100)$$

leads to an expression for v at time 0:

$$v(0) = \frac{\frac{r}{1+r}}{\frac{r}{1+r} + T^2} v(T) - 2y \frac{r}{(1+r)^2} \int_T^0 \frac{t}{(\frac{r}{1+r} + t^2)^2} dt + \frac{r}{1+r} \int_T^0 \frac{\sqrt{2t}}{\frac{r}{1+r} + t^2} d\bar{\beta}_t. \quad (101)$$

Using the change-of-variable, $s = \frac{r}{1+r} + t^2$, one can show that

$$2 \int_T^0 \frac{t}{(\frac{r}{1+r} + t^2)^2} dt = -\frac{T^2}{\frac{r}{1+r}(\frac{r}{1+r} + T^2)}. \quad (102)$$

Using this result in (101) simplifies the expression to

$$v(0) = \frac{\frac{r}{1+r}}{\frac{r}{1+r} + T^2} v(T) + \frac{r}{(1+r)^2} \frac{T^2}{\frac{r}{1+r}(\frac{r}{1+r} + T^2)} y + \frac{r}{1+r} \int_T^0 \frac{\sqrt{2t}}{\frac{r}{1+r} + t^2} d\bar{\beta}_t, \quad (103)$$

which is the desired result.

C Solution to the SDE in (50)

To solve the SDE

$$dv = -\frac{2}{t} \left[\frac{\frac{\alpha^j r}{\alpha^j + r}}{\frac{\alpha^j r}{\alpha^j + r} + t^2} (v - \bar{x}) + \frac{\frac{\alpha^j t^2}{\alpha^j + r}}{\frac{\alpha^j r}{\alpha^j + r} + t^2} (y - \bar{x}) - (v - \bar{x}) \right] dt + \sqrt{2t} d\bar{\beta}_t, \quad (104)$$

we re-write it as

$$dv = -\frac{2}{t} \left[-\frac{t^2}{\frac{\alpha^j r}{\alpha^j + r} + t^2} (v - \bar{x}) + \frac{\frac{\alpha^j t^2}{\alpha^j + r}}{\frac{\alpha^j r}{\alpha^j + r} + t^2} (y - \bar{x}) \right] dt + \sqrt{2t} d\bar{\beta}_t, \quad (105)$$

and use the change of variables $v' = v - \bar{x}$ to obtain

$$dv' - 2t \frac{1}{\frac{\alpha^j r}{\alpha^j + r} + t^2} v' dt = -2t \frac{\frac{\alpha^j}{\alpha^j + r}}{\frac{\alpha^j r}{\alpha^j + r} + t^2} (y - \bar{x}) dt + \sqrt{2t} d\bar{\beta}_t. \quad (106)$$

A few simple manipulations yield

$$\frac{1}{\frac{\alpha^j r}{\alpha^j + r} + t^2} dv' - 2t \frac{1}{(\frac{\alpha^j r}{\alpha^j + r} + t^2)^2} v' dt = -2t \frac{\frac{\alpha^j}{\alpha^j + r}}{(\frac{\alpha^j r}{\alpha^j + r} + t^2)^2} (y - \bar{x}) dt + \frac{\sqrt{2t}}{\frac{\alpha^j r}{\alpha^j + r} + t^2} d\bar{\beta}_t, \quad (107)$$

$$d\left(\frac{1}{\frac{\alpha^j r}{\alpha^j + r} + t^2} v'\right) = -2t \frac{\frac{\alpha^j}{\alpha^j + r}}{(\frac{\alpha^j r}{\alpha^j + r} + t^2)^2} (y - \bar{x}) dt + \frac{\sqrt{2t}}{\frac{\alpha^j r}{\alpha^j + r} + t^2} d\bar{\beta}_t. \quad (108)$$

Integrating backwards in time, from T to 0,

$$\int_T^0 d\left(\frac{1}{\frac{\alpha^j r}{\alpha^j + r} + t^2} v'(t)\right) = -2(y - \bar{x}) \int_T^0 \frac{\frac{\alpha^j}{\alpha^j + r} t}{(\frac{\alpha^j r}{\alpha^j + r} + t^2)^2} dt + \int_T^0 \frac{\sqrt{2t}}{\frac{\alpha^j r}{\alpha^j + r} + t^2} d\bar{\beta}_t, \quad (109)$$

yields

$$v'(0) = \frac{\frac{\alpha^j r}{\alpha^j + r}}{\frac{\alpha^j r}{\alpha^j + r} + T^2} v'(T) - 2(y - \bar{x}) \frac{(\alpha^j)^2 r}{(\alpha^j + r)^2} \int_T^0 \frac{t}{(\frac{\alpha^j r}{\alpha^j + r} + t^2)^2} dt + \frac{\alpha^j r}{\alpha^j + r} \int_T^0 \frac{\sqrt{2t}}{\frac{\alpha^j r}{\alpha^j + r} + t^2} d\bar{\beta}_t. \quad (110)$$

Making use of (102) gives us

$$v'(0) = \frac{\frac{\alpha^j r}{\alpha^j + r}}{\frac{\alpha^j r}{\alpha^j + r} + T^2} v'(T) + \frac{(\alpha^j)^2 r}{(\alpha^j + r)^2} \frac{T^2}{\frac{\alpha^j r}{\alpha^j + r} (\frac{\alpha^j r}{\alpha^j + r} + T^2)} (y - \bar{x}) + \frac{\alpha^j r}{\alpha^j + r} \int_T^0 \frac{\sqrt{2t}}{\frac{\alpha^j r}{\alpha^j + r} + t^2} d\bar{\beta}_t. \quad (111)$$

Undoing the change of variables finally yields

$$v(0) = \bar{x} + \frac{\frac{\alpha^j r}{\alpha^j + r}}{\frac{\alpha^j r}{\alpha^j + r} + T^2} (v(T) - \bar{x}) + \frac{(\alpha^j)^2 r}{(\alpha^j + r)^2} \frac{T^2}{\frac{\alpha^j r}{\alpha^j + r} (\frac{\alpha^j r}{\alpha^j + r} + T^2)} (y - \bar{x}) + \frac{\alpha^j r}{\alpha^j + r} \int_T^0 \frac{\sqrt{2t}}{\frac{\alpha^j r}{\alpha^j + r} + t^2} d\bar{\beta}_t, \quad (112)$$

which is the desired result.

References

- Adrian, M., D. Sanz-Alonso, and W. R., 2025: Data assimilation with machine learning surrogate models: A case study with FourCastNet. *Artificial Intelligence for Earth System*.
- Allen, A., and Coauthors, 2025: End-to-end data-driven weather prediction. *Nature*, <https://doi.org/https://doi.org/10.1038/s41586-025-08897-0>.
- Anderson, B. D., 1982: Reverse-time diffusion equation models. *Stochastic Processes and their Applications*, **12** (3), 313–326, [https://doi.org/https://doi.org/10.1016/0304-4149\(82\)90051-5](https://doi.org/https://doi.org/10.1016/0304-4149(82)90051-5), URL <https://www.sciencedirect.com/science/article/pii/0304414982900515>.
- Anderson, J., 2001: An ensemble adjustment Kalman filter for data assimilation. *Monthly weather review*, **129** (12), 2884–2903.

- Bao, F., Z. Zhang, and G. Zhang, 2024: A score-based filter for nonlinear data assimilation. *Journal of Computational Physics*, **514**, 113 207, <https://doi.org/10.1016/j.jcp.2024.113207>, URL <https://www.sciencedirect.com/science/article/pii/S002199912400456X>.
- Batzolis, G., J. Stanczuk, C.-B. Schönlieb, and C. Etmann, 2021: Conditional image generation with score-based diffusion models. URL <https://arxiv.org/abs/2111.13606>, 2111.13606.
- Bengtsson, T., P. Bickel, and B. Li, 2008: Curse of dimensionality revisited: The collapse of importance sampling in very large scale systems. *IMS Collections: Probability and Statistics: Essays in Honor of David A. Freedman*, **2**, 316–334.
- Bickel, P., T. Bengtsson, and J. Anderson, 2008: Sharp failure rates for the bootstrap particle filter in high dimensions. *Pushing the Limits of Contemporary Statistics: Contributions in Honor of Jayanta K. Ghosh*, **3**, 318–329.
- Buehner, M., J. Mounneau, and C. Charette, 2013: Four-dimensional ensemble-variational data assimilation for global deterministic weather prediction. *Nonlin. Processes Geophys.*, **20**, 669–682.
- Burgers, G., P. V. Leeuwen, and G. Evensen, 1998: Analysis scheme in the ensemble Kalman filter. *Monthly weather review*, **126** (6), 1719–1724.
- Chung, H., J. Kim, M. T. Mccann, M. L. Klasky, and J. C. Ye, 2023: Diffusion posterior sampling for general noisy inverse problems. *The Eleventh International Conference on Learning Representations*, URL <https://arxiv.org/abs/2209.14687>.
- Ding, X., Y. Wang, K. Zhang, and Z. J. Wang, 2025: CCDM: Continuous conditional diffusion models for image generation. URL <https://arxiv.org/abs/2405.03546>, 2405.03546.
- Efron, B., 2011: Tweedie’s formula and selection bias. *Journal of the American Statistical Association*, **106**(496), 1602–1614.
- Evensen, G., 1994: Sequential data assimilation with a nonlinear quasi-geostrophic model using Monte Carlo methods to forecast error statistics. *Journal of Geophysical Research: Oceans*, **99** (C5), 10 143–10 162, <https://doi.org/10.1029/94JC00572>.
- Evensen, G., and Coauthors, 2009: *Data assimilation: the ensemble Kalman filter*, Vol. 2. Springer.
- Gharamti, M. E., K. Raeder, J. Anderson, and X. Wang, 2019: Comparing adaptive prior and posterior inflation for ensemble filters using an atmospheric general circulation model. *Monthly Weather Review*, **147** (7), 2535 – 2553, <https://doi.org/10.1175/MWR-D-18-0389.1>, URL <https://journals.ametsoc.org/view/journals/mwre/147/7/mwr-d-18-0389.1.xml>.
- Hamill, T. M., and C. Snyder, 2000: A hybrid ensemble Kalman filter-3D variational analysis scheme. *Monthly Weather Review*, **128**, 2905–2919.
- Ho, J., A. Jain, and P. Abbeel, 2020: Denoising diffusion probabilistic models. *34th Conference on Neural Information Processing Systems (NeurIPS 2020)*, URL <https://proceedings.neurips.cc/paper/2020/file/4c5bcfec8584af0d967f1ab10179ca4b-Paper.pdf>.
- Hodyss, D., W. F. Campbell, and J. S. Whitaker, 2016: Observation-dependent posterior inflation for the ensemble Kalman filter. *Monthly Weather Review*, **144**, 2667–2684.
- Hodyss, D., and M. Morzfeld, 2023: How sampling errors in covariance estimates cause bias in the Kalman gain and impact ensemble data assimilation. *Monthly Weather Review*, **151** (9),

- 2413 – 2426, <https://doi.org/10.1175/MWR-D-23-0029.1>, URL <https://journals.ametsoc.org/view/journals/mwre/151/9/MWR-D-23-0029.1.xml>.
- Huang, L., L. Gianinazzi, Y. Yu, P. D. Dueben, and T. Hoefler, 2024: Diffda: a diffusion model for weather-scale data assimilation. URL <https://arxiv.org/abs/2401.05932>, 2401.05932.
- Kalnay, E., 2002: *Atmospheric Modeling, Data Assimilation and Predictability*. Cambridge University Press.
- Karras, T., M. Aittala, T. Aila, and S. Laine, 2022: Elucidating the design space of diffusion-based generative models. *36th Conference on Neural Information Processing Systems*, **35**, 26 565–26 577.
- Keller, J. D., and R. Potthast, 2024: AI-based data assimilation: Learning the functional of analysis estimation. URL <https://arxiv.org/abs/2406.00390>, 2406.00390.
- Kochkov, D., and Coauthors, 2024: Neural general circulation models for weather and climate. *Nature*, **632**, 1060–1066.
- Kuhl, D. D., T. E. Rosmond, C. H. Bishop, J. McLay, and N. L. Baker, 2013: Comparison of hybrid ensemble/4dvar and 4dvar within the navdas-ar data assimilation framework. *Monthly Weather Review*, **141**, 2740–2758.
- Lam, R., and Coauthors, 2023: Learning skillful medium-range global weather forecasting. *Science*, **382** (6677), 1416–1421, <https://doi.org/10.1126/science.adi2336>, URL <https://www.science.org/doi/abs/10.1126/science.adi2336>, <https://www.science.org/doi/pdf/10.1126/science.adi2336>.
- Li, L., R. Carver, I. Lopez-Gomez, F. Sha, and J. Anderson, 2024: Generative emulation of weather forecast ensembles with diffusion models. *Science Advances*, **10** (13), eadk4489, <https://doi.org/10.1126/sciadv.adk4489>, URL <https://www.science.org/doi/abs/10.1126/sciadv.adk4489>, <https://www.science.org/doi/pdf/10.1126/sciadv.adk4489>.
- Li, Z., B. Dong, and P. Zhang, 2025: State-observation augmented diffusion model for nonlinear assimilation with unknown dynamics. URL <https://arxiv.org/abs/2407.21314>, 2407.21314.
- Lorenc, A., 2003: The potential of the ensemble Kalman filter for NWP – a comparison with 4D-Var. *Quarterly Journal of the Royal Meteorological Society*, **129** (595), 3183–3203, <https://doi.org/10.1256/qj.02.132>.
- Manshausen, P., and Coauthors, 2024: Generative data assimilation of sparse weather station observations at kilometer scales. URL <https://arxiv.org/abs/2406.16947>, 2406.16947.
- Mardani, M., and Coauthors, 2025: Residual corrective diffusion modeling for km-scale atmospheric downscaling. *Commun Earth Environ*, **6**, <https://doi.org/10.1038/s43247-025-02042-5>.
- Morzfeld, M., and D. Hodyss, 2019: Gaussian approximations in filters and smoothers for data assimilation. *Tellus A: Dynamic Meteorology and Oceanography*, **71** (1), 1600 344, <https://doi.org/10.1080/16000870.2019.1600344>.
- Morzfeld, M., and D. Hodyss, 2023: A theory for why even simple covariance localization is so useful in ensemble data assimilation. *Monthly Weather Review*, **151**, 717–736.

- Parthasarathy, V. B., A. Zafar, A. Khan, and A. Shahid, 2024: The ultimate guide to fine-tuning llms from basics to breakthroughs: An exhaustive review of technologies, research, best practices, applied research challenges and opportunities. URL <https://arxiv.org/abs/2408.13296>, 2408.13296.
- Pathak, J., and Coauthors, 2024: Kilometer-scale convection allowing model emulation using generative diffusion modeling. URL <https://arxiv.org/abs/2408.10958>, 2408.10958.
- Poterjoy, J., and F. Zhang, 2015: Systematic comparison of four-dimensional data assimilation methods with and without the tangent linear model using hybrid background error covariance: E4DVar versus 4DEnVar. *Monthly Weather Review*, **143** (5), 1601–1621.
- Price, I., and Coauthors, 2025: Probabilistic weather forecasting with machine learning. *Nature*, **637**, 84–90.
- Qu, Y., J. Nathaniel, S. Li, and P. Gentine, 2024: Deep Generative Data Assimilation in Multimodal Setting . *2024 IEEE/CVF Conference on Computer Vision and Pattern Recognition Workshops (CVPRW)*, IEEE Computer Society, Los Alamitos, CA, USA, 449–459, <https://doi.org/10.1109/CVPRW63382.2024.00050>, URL <https://doi.ieeecomputersociety.org/10.1109/CVPRW63382.2024.00050>.
- Rozet, F., and G. Louppe, 2023: Score-based data assimilation. *Thirty-seventh Conference on Neural Information Processing Systems*, URL <https://openreview.net/forum?id=VUvLSnMZdX>.
- Snyder, C., T. Bengtsson, P. Bickel, and J. Anderson, 2008: Obstacles to high-dimensional particle filtering. *Monthly Weather Review*, **136** (12), 4629–4640.
- Snyder, C., T. Bengtsson, and M. Morzfeld, 2015: Performance bounds for particle filters using the optimal proposal. *Monthly Weather Review*, **143**, 4750–4761.
- Sohl-Dickstein, J., E. Weiss, N. Maheswaranathan, and S. Ganguli, 2015: Deep unsupervised learning using nonequilibrium thermodynamics. *Proceedings of the 32nd International Conference on Machine Learning*, F. Bach, and D. Blei, Eds., PMLR, Lille, France, Proceedings of Machine Learning Research, Vol. 37, 2256–2265, URL <https://proceedings.mlr.press/v37/sohl-dickstein15.html>.
- Talagrand, O., and P. Courtier, 1987: Variational assimilation of meteorological observations with the adjoint vorticity equation. i: Theory. *Quarterly Journal of the Royal Meteorological Society*, **113** (478), 1311–1328.
- Tippett, M., J. Anderson, C. Bishop, T. Hamill, and J. Whitaker, 2003: Ensemble square root filters. *Monthly Weather Review*, **131** (7), 1485 – 1490, [https://doi.org/10.1175/1520-0493\(2003\)131<1485:ESRF>2.0.CO;2](https://doi.org/10.1175/1520-0493(2003)131<1485:ESRF>2.0.CO;2).
- van Leeuwen, P. J., 2020: A consistent interpretation of the stochastic version of the ensemble kalman filter. *Quarterly Journal of the Royal Meteorological Society*, **146** (731), 2815–2825, <https://doi.org/https://doi.org/10.1002/qj.3819>, URL <https://rmets.onlinelibrary.wiley.com/doi/abs/10.1002/qj.3819>, <https://rmets.onlinelibrary.wiley.com/doi/pdf/10.1002/qj.3819>.
- Whitaker, J. S., and T. M. Hamill, 2012: Evaluating methods to account for system errors in ensemble data assimilation. *Mon. Wea. Rev.*, **140**, 3078–3089.
- Zhan, Z., D. Chen, J.-P. Mei, Z. Zhao, J. Chen, C. Chen, S. Lyu, and C. Wang, 2024: Conditional

- image synthesis with diffusion models: A survey. *CoRR*, **abs/2409.19365**, URL <https://doi.org/10.48550/arXiv.2409.19365>.
- Zhang, F., M. Zhang, and J. A. Hansen, 2009: Coupling ensemble Kalman filter with four-dimensional variational data assimilation. *Advances in Atmospheric Sciences*, **26**, 1–8.
- Zhuang, F., Z. Qi, K. Duan, D. Xi, Y. Zhu, H. Zhu, H. Xiong, and Q. He, 2020: A comprehensive survey on transfer learning. URL <https://arxiv.org/abs/1911.02685>, 1911.02685.